

Physicochemical Targeting of Lipid Nanoparticles to the Lungs Induces Clotting: Mechanisms and Solutions

Serena Omo-Lamai, Marco E. Zamora, Manthan N. Patel, Jichuan Wu, Jia Nong, Zhicheng Wang, Alina Peshkova, Aparajeeta Majumder, Jilian R. Melamed, Liam S. Chase, Eno-Obong Essien, Drew Weissman, Vladimir R. Muzykantov, Oscar A. Marcos-Contreras,* Jacob W. Myerson,* and Jacob S. Brenner*

Lipid nanoparticles (LNPs) have become the dominant drug delivery technology in industry, holding the promise to deliver RNA to up or down-regulate any protein of interest. LNPs have mostly been targeted to specific cell types or organs by physicochemical targeting in which LNP's lipid compositions are adjusted to find mixtures with the desired tropism. Here lung-tropic LNPs are examined, whose organ tropism derives from containing either a cationic or ionizable lipid conferring a positive zeta potential. Surprisingly, these LNPs are found to induce massive thrombosis. Such thrombosis is shown in the lungs and other organs, and it is shown that it is greatly exacerbated by pre-existing inflammation. This clotting is induced by a variety of formulations with cationic lipids, including LNPs and non-LNP nanoparticles, and even by lung-tropic ionizable lipids that do not have a permanent cationic charge. The mechanism depends on the LNPs binding to and then changing the conformation of fibrinogen, which then activates platelets and thrombin. Based on these mechanisms, multiple solutions are engineered that enable positively charged LNPs to target the lungs while ameliorating thrombosis. The findings illustrate how physicochemical targeting approaches must be investigated early for risks and re-engineered with a careful understanding of biological mechanisms.

1. Introduction

Since the first Food and Drug Administration (FDA) approval of a solid LNP in 2018, LNPs have rapidly become the preferred drug delivery platform of the biopharma industry, with the trend accelerating markedly after the development of the COVID-19 LNP vaccines.^[1] Targeting LNPs to specific organs or cell types is desirable for many applications and is generally accomplished by one of two methods. The older method is to conjugate LNPs to affinity moieties (e.g., antibodies) that bind to a known epitope on a target cell.^[2] This method presents major challenges for scale-up manufacturability and immunogenicity, partially contributing to it never having produced an FDA-approved targeted LNP or liposome. The second, and newer, method for LNP targeting is to screen large numbers of LNP formulations for those that have fortuitous “physicochemical tropism” to a target organ. In physicochemical tropism/targeting,

S. Omo-Lamai, L. S. Chase
 Department of Bioengineering
 University of Pennsylvania
 Philadelphia, PA 19104, USA

M. E. Zamora
 School of Biomedical Engineering
 Drexel University
 Philadelphia, PA 19104, USA

M. E. Zamora, M. N. Patel, J. Nong, Z. Wang, A. Peshkova, A. Majumder, E.-O. Essien, V. R. Muzykantov, O. A. Marcos-Contreras, J. W. Myerson, J. S. Brenner
 Department of Systems Pharmacology and Translational Therapeutics
 Perelman School of Medicine
 University of Pennsylvania
 Philadelphia, PA 19104, USA
 E-mail: oscarmar@penmedicine.upenn.edu myerson@penmedicine.upenn.edu jacob.brenner@penmedicine.upenn.edu

J. Wu, J. S. Brenner
 Division of Pulmonary Allergy, and Critical Care
 Department of Medicine
 Perelman School of Medicine
 University of Pennsylvania
 Philadelphia, PA 19104, USA
 J. R. Melamed, D. Weissman
 Department of Medicine
 Perelman School of Medicine
 University of Pennsylvania
 Philadelphia, PA 19104, USA

 The ORCID identification number(s) for the author(s) of this article can be found under <https://doi.org/10.1002/adma.202312026>

© 2024 The Authors. Advanced Materials published by Wiley-VCH GmbH. This is an open access article under the terms of the [Creative Commons Attribution-NonCommercial](https://creativecommons.org/licenses/by-nc/4.0/) License, which permits use, distribution and reproduction in any medium, provided the original work is properly cited and is not used for commercial purposes.

DOI: 10.1002/adma.202312026

some (usually unknown) physical or chemical features of the LNP cause it to enter into particular cells. Over the last decade, the physicochemical approach has become the dominant method of achieving targeting in both academia and industry, because of the ease of in vivo screening and the highly efficient manufacturing process. As physicochemical tropism has been able to target many different organs and cell types, it has the potential to meet LNPs' promise of being able to modulate any protein in any cell type or organ.

Physicochemical targeting is usually achieved by screening many lipids, typically varying each of the four major lipid classes used in LNPs: ionizable lipids, PEGylated lipids, cholesterol, and helper lipids (phospholipids, sphingolipids, etc). The mechanisms of targeting are rarely elucidated. As a notable exception, ApoE was implicated as the plasma protein that binds to the first FDA-approved LNP, patisiran, shuttling the LNPs to hepatocytes.^[3,4] While mechanisms of delivery generally are not elucidated, there have been some clear trends in physicochemical properties that correlate with organ distribution. For example, intravenously injected (IV) LNPs formulated with negatively charged lipids often accumulate in the spleen^[5–9] and LNPs formulated with positively charged lipids usually accumulate in the lungs^[5,7,9–12] as found independently by many labs and companies. These observations were, in a 2020 *Nature Nanotechnology* paper, distilled into a simpler and more elegant way of targeting LNPs.^[5] Instead of using particular ratios of hard-to-synthesize ionizable lipids or exotic helper lipids, this seminal study showed it was possible to add to a base formulation of LNPs either a negatively charged lipid to target the spleen or a positively charged lipid to target the lungs. This approach leads to democratization and reproducibility since any lab or company can obtain such common lipids, rather than having to synthesize the ionizable lipid variants used in a particular lab's screening.

However, while testing such promising physicochemically-targeted LNPs as therapeutics, we found that the positively charged LNPs with lung tropism induce a major unreported side effect: thrombosis. Studies of nanoparticle toxicities have largely focused on two of the three major defense systems of plasma: complement proteins and immunoglobulins.^[13–15] However, the 3rd defense system, clotting, has often been neglected in recent years, even though it has the most deadly and acute consequences if improperly activated. Blood has evolved to actively clot in response to different foreign surfaces and the coagulation cascade is specifically known to activate in response to charged surfaces. An IV dose of nanoparticles exposes the blood to large amounts of foreign surface area, but nanoparticles can also indirectly activate clotting by interacting with cells that affect clotting processes, such as endothelial cells, neutrophils, and platelets. Noting that the dominant nanomedicine targeting method now employs manipulation of nanoparticle charge, it is important to revisit the thrombotic side effects of nanomedicines^[16–21] with a focus on the new targeting approaches.

Here, we show that lung tropic, positively charged, LNPs induce massive thrombosis. This finding was quite general, as it held for LNPs with different permanently positively charged lipids, regardless of their co-loaded ionizable lipid, and not just LNPs, but also liposomes. Perhaps most surprisingly, we also observed thrombosis caused by LNPs that lacked a permanently cationic lipid (one possessing a quaternary amine) but instead

contained an ionizable lipid (possessing a tertiary amine) that was found via screening to confer lung tropism. The lung-tropic LNPs induced profound pulmonary embolism when administered intravenously, induced stroke-like effects when administered via the carotid artery, and modified clotting processes in ex vivo blood. We investigated detailed mechanisms of LNP-induced clotting, showing that lung-tropic LNPs bind to the core clotting protein, fibrinogen, alter its secondary structure, and cause aggregation and activation of platelets. Elucidating these detailed mechanisms of clotting enabled us to develop three solutions that may permit positively charged LNPs to maintain their lung-targeting property while ameliorating dangerous clotting: Pre-treatment with anticoagulants (direct thrombin inhibitors, but not the seemingly obvious choice of heparin), conjugation of the LNPs to direct thrombin inhibitors, or reduction of the LNP size.

2. Results

2.1. Lung-Tropic LNPs with Cationic Lipids Induce Gross Side Effects In Vivo

We fabricated physicochemically-targeted, lung-tropic LNPs by the previously published method of adding in a cationic lipid, 1,2-dioleoyl-3-trimethylammonium-propane (DOTAP, chloride salt). We initially synthesized these LNPs with the ionizable lipid cKK-E12 (herein referred to as +DOTAP LNPs, unless otherwise stated). This base +DOTAP LNP formulation consisted of the lipids DOTAP, cKK-E12, 1,2-dioleoyl-*sn*-glycero-3-phosphoethanolamine (DOPE), cholesterol, 1,2-dimyristoyl-rac-glycero-3-methoxypolyethylene glycol-2000 (DMG-PEG 2000) (50/25/5/18.5/1.5, mol/mol) and mRNA (lipid/mRNA ratio = 40/1, wt/wt). Control, non-lung tropic LNPs were synthesized without DOTAP (**Figure 1a**). There was no significant difference in the sizes of these LNPs (99.22 ± 4.27 nm for –DOTAP LNPs and 102.47 ± 0.48 nm for +DOTAP LNPs) (**Figure 1b**). However, +DOTAP LNPs had a significantly higher zeta potential than –DOTAP LNPs (14.34 mV vs –4.05 mV) due to the addition of the cationic lipid (**Figure 1c**).

We next intravenously (IV) injected the above LNPs into naive mice at a dose of 10 μ g of mRNA per mouse and sacrificed 30 min later for gross anatomical inspection. We observed that in mice that received +DOTAP LNPs, the lungs were strikingly red and firm, resembling “hepatization” (liver-like appearance) described by pathologists for human acute respiratory distress syndrome (ARDS) (**Figure 1d**). We observed clear lethargy and sluggishness in +DOTAP LNP mice. Using the software DeepLabCut as previously described,^[22] we found that after a recording time interval of 1 h post-LNP injection, +DOTAP LNP mice walked a total distance that was > 17-fold less than naive mice (**Figure 1e**). We further assessed lung-specific toxicity by measuring the contents of the bronchoalveolar lavage (BAL) fluid 20 h after IV +DOTAP LNP injection, which assesses lung capillary leak. In naive mice, there was a dose-dependent increase in both BAL protein and leukocyte count from 5 to 10 μ g of mRNA (**Figure 1f** and **Figure S1**, Supporting Information).

Because lung-targeted LNPs will generally be given to patients with lung pathology, we next investigated whether +DOTAP LNPs caused even more severe injury in mice with pre-existing lung inflammation. We utilized a mouse model of acute lung

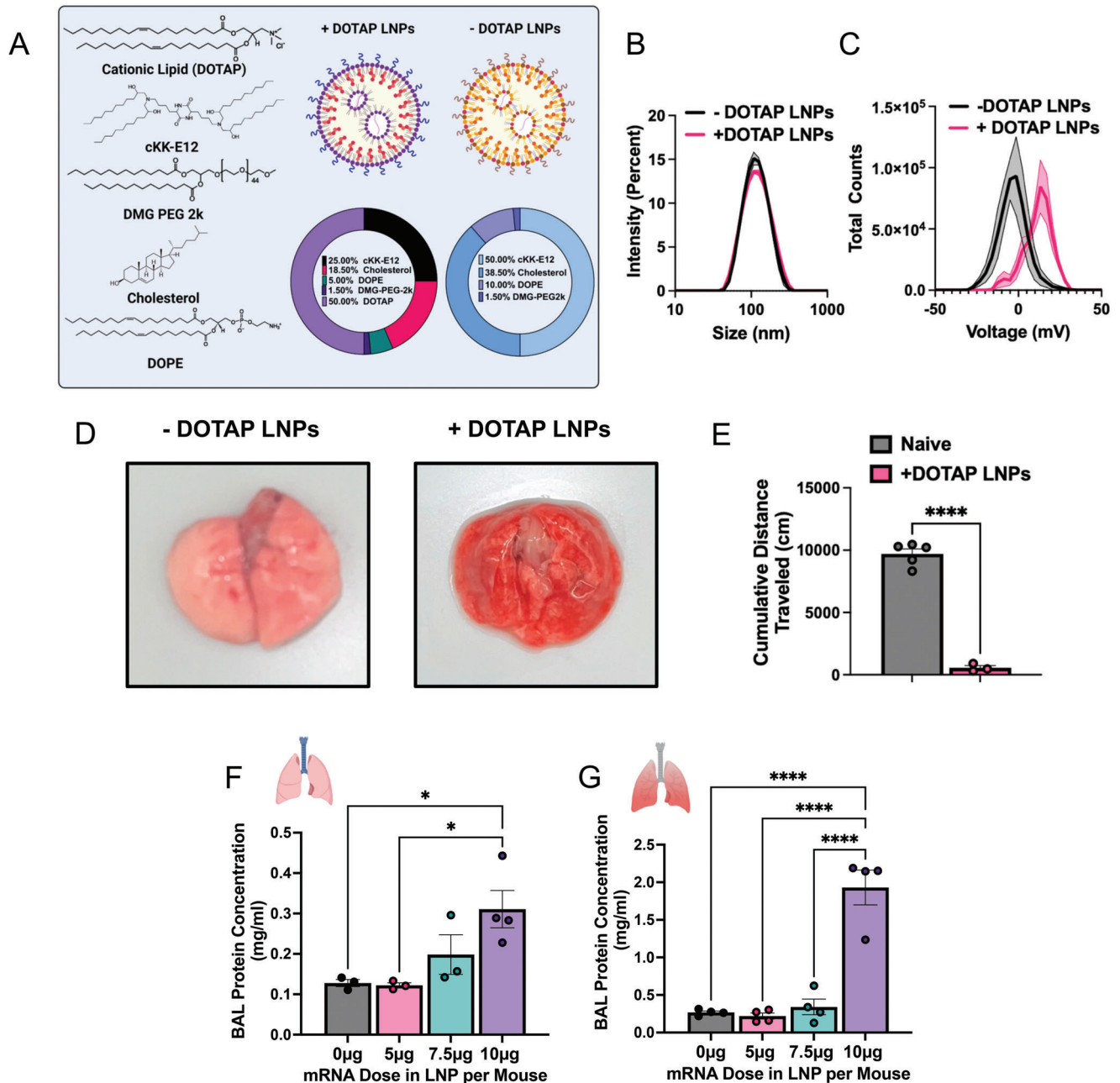


Figure 1. Cationic LNPs with physicochemical tropism to the lungs induce acute, severe side effects in mice. A) Formulation of -DOTAP and +DOTAP LNPs. B) Size distribution of -DOTAP and +DOTAP LNPs determined by dynamic light scattering (DLS) shows no significant difference in size (99.22 ± 4.27 nm for -DOTAP LNPs and 102.47 ± 0.48 nm for +DOTAP LNPs). C) Zeta potential graphs of -DOTAP LNP (black) versus +DOTAP LNP (pink), show that -DOTAP LNPs are slightly negatively charged at -4.05 mV and +DOTAP LNPs have a surface charge of 14.34 mV. D) Gross anatomical comparison of naive mice intravenously (IV) injected with either -DOTAP LNPs or +DOTAP LNPs reveals severe lung hepatization (liver-like appearance) with +DOTAP LNP injected mice. LNPs were allowed to circulate for 30 min. E) Comparison of cumulative distance traveled for 1 h after injection of +DOTAP LNPs assessed by AI software, DeepLabCut, compared to healthy, uninjected mice reveals a significant reduction in total distance traveled, indicating lethargy in these mice. F) Dose-response of the effect of +DOTAP LNP dose on protein concentration in bronchoalveolar lavage (BAL) fluid shows a dose-dependent increase in BAL protein, a measure of endothelial barrier dysfunction. G) This is further exacerbated in mice with pre-existing lung inflammation (nebulized LPS mice; note the 5-fold y-axis augmentation between (F) and (G)). Statistics: $n = 3-5$ and data shown represents mean \pm SEM; For (E), comparisons between groups were made using an unpaired t -test with Welch's correction. For all other graphs, comparisons between groups were made using one-way ANOVA with Tukey's post-hoc test. * = $p < 0.05$, ** = $p < 0.001$, **** = $p < 0.0001$.

inflammation achieved by administering nebulized lipopolysaccharides (LPS). +DOTAP LNPs were IV injected 4 h after LPS exposure and mice were sacrificed 20 h later. As in naïve mice, we saw a dose-dependent increase in BAL protein concentration from 5 to 10 µg of mRNA (Figure 1g).

However, in nebulized LPS mice, there was an exacerbation of BAL edema at each dose tested. At the 10 µg dose of mRNA, nebulized LPS mice have 6-fold higher BAL edema compared to naïve mice injected with +DOTAP LNPs. This indicates that the toxicity of +DOTAP LNPs is amplified under pre-existing inflammatory conditions. Based on these data, a dose of 10 µg of mRNA in LNPs was used for further in vivo studies unless otherwise stated. This is a therapeutically relevant dose for mRNA-LNP delivery and enabled us to adequately assess the mechanisms behind DOTAP LNP toxicity.

2.2. Coagulation is Triggered by LNPs and Other Nanoparticles with Cationic Lipids, across Diverse Formulations

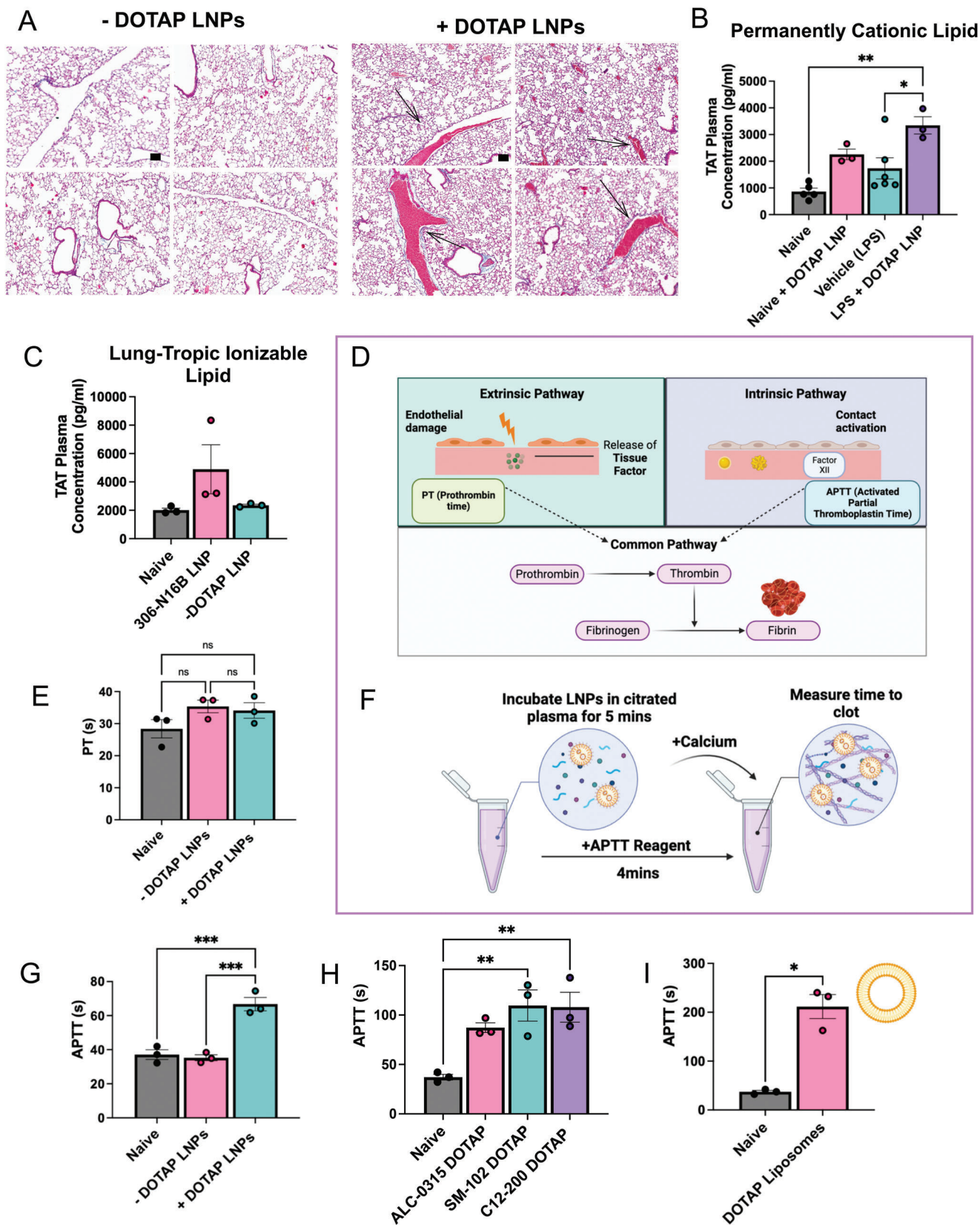
Given the very acute nature of the side effects of +DOTAP LNPs, seen within a minute on the AI-measured distance-walked test, we hypothesized that the nanoparticles were activating a protein-based defense system in the blood. The three major plasma protein defense systems are the complement cascade, immunoglobulins, and the coagulation cascade. Since complement has been long implicated in nanoparticle defense,^[13–15] and since immunoglobulins' acute effects also lead to complement activation (via IgG-mediated activation of the classical pathway of complement), we first investigated if these LNPs activate the complement system. Surprisingly, we discovered that +DOTAP LNPs do not activate complement, as we detected no increase in the plasma concentration of C3a 30 min after +DOTAP LNP IV injection into naïve mice (Figure S2, Supporting Information), noting that we have extensively shown C3a production induced by other nanoparticles^[13,14] Without C3a production, it is highly unlikely that complement activation, or acute immunoglobulin effects, mediate +DOTAP LNPs' acute toxicity.

Therefore, we investigated whether the toxicity was produced by the coagulation cascade. To investigate this, we stained lung sections with Masson's trichrome to look for evidence of clots. Lung histological samples show large clots both at the large vessel and capillary levels in naïve mice IV injected with +DOTAP LNPs, compared to mice injected with –DOTAP LNPs where there are no observable clots (Figure 2a). This was a clear indication of thrombosis (clotting) due to +DOTAP LNPs. In these mice, visible clots were not observed in the liver or the spleen (Figure S3a,b, Supporting Information). However, this effect is not restricted to the lungs since we also observed evidence of clotting in the brain when +DOTAP LNPs were injected via the carotid artery (Figure S3c, Supporting Information). These results indicate the incidence of clots in the first capillary bed downstream of injection (lungs after IV injection; brain after intra-arterial injection). To quantify the extent of clotting, we measured thrombin-antithrombin (TAT) plasma levels in both naïve and nebulized-LPS injured mice. TAT is a stable complex formed after thrombin activation that serves as a marker of coagulation. We found that +DOTAP LNPs increase TAT levels by > 2-fold in

naïve mice and by an additional > 1.5-fold in nebulized-LPS injured mice (Figure 2b). This confirmed that +DOTAP LNPs activate thrombin (the common pathway of coagulation), and this is exacerbated in pre-existing inflammatory conditions, probably as a result of thrombo-inflammation.^[23] Furthermore, we show that in addition to permanently cationic lipids like DOTAP, ionizable cationic lipids that are used to induce lung tropism also induce clotting. An example of such an ionizable lipid is 306-N16B, which was shown in a recent PNAS paper to produce excellent lung tropism^[24] and is also cationic at neutral pH (Figure S4 and Table S1, Supporting Information). However, we found that 306-N16B LNPs also increase TAT plasma levels by ≈2.5-fold in naïve mice (Figure 2c) and demonstrate other indications of coagulation (Figure S5, Supporting Information). This finding therefore generalizes this clotting phenomenon to a wide variety of physicochemically-targeted LNPs that rely on positive charge for lung localization.

We sought to determine which molecular coagulation pathways underlie LNP-induced thrombosis. Coagulation can be divided into the intrinsic and extrinsic pathways (Figure 2d). The extrinsic pathway is activated by trauma that damages the endothelium, leading to exposure of tissue factor which activates the coagulation protein factor VII. The intrinsic pathway is initiated by factors within the blood vessel lumen and has been shown to be triggered by charged surfaces (such as foreign particles) or collagen, which trigger the activation of the coagulation protein factor XII.^[25] The extrinsic and intrinsic pathways converge to the common pathway which involves the conversion of prothrombin to thrombin – the enzyme that converts fibrinogen to fibrin. Fibrin forms the mesh-like framework of clots. The prothrombin time (PT) and activated partial thromboplastin time (APTT) are laboratory tests used to measure the time to clot through either the extrinsic or intrinsic pathways, respectively. To determine if +DOTAP LNP-activated coagulation employs the intrinsic or extrinsic pathway, we measured PT and APTT after dosing LNPs into plasma in vitro. While +DOTAP LNPs did not change the PT (Figure 2e), they led to a significant increase in APTT (Figure 2f,g). This indicates that +DOTAP LNPs activate the intrinsic coagulation pathway, thus depleting intrinsic pathway proteins and prolonging the APTT. Furthermore, the effects of +DOTAP LNPs on coagulation are dependent on both the number of LNPs injected and the mole fraction of DOTAP in the formulation (Figure S6b,d,e, Supporting Information).

We formulated liposomes and other LNPs with DOTAP to see if the coagulation side effects were a generalizable result of co-formulation with cationic lipids. We formulated LNPs with various ionizable lipids (C12-200, ALC-0315, SM-102; Figure S4 and Table S1, Supporting Information) and found that +DOTAP LNPs increase APTT, regardless of the ionizable lipid type (Figure 2h). We used DOTMA, rather than DOTAP, as our cationic lipid and observed the same effect on APTT (Figure S7, Supporting Information). Adding DOTAP to liposomes, rather than LNPs, also results in increased APTT (Figure 2i and Figure S8a, Supporting Information). Finally, 306-N16B LNPs also lead to an increase in clotting time in vivo (Figure S5d, Supporting Information). Thus, this clotting phenomenon is generalizable to different LNP and liposome formulations containing both ionizable and permanently cationic lipids. Notably, these side effects appear to be associated with a positive charge as anionic LNPs



formulated with the negatively charged lipid DOPS do not induce clotting (Figure S8b,c, Supporting Information).

2.3. LNPs with Cationic Lipids Aggregate and Activate Platelets

Having proven that +DOTAP LNPs activate the coagulation cascade, we sought to assess if +DOTAP LNPs also cause activation and aggregation of platelets, since clots can also form due to platelet aggregates.^[26] We measured complete blood counts (CBCs) in blood drawn 30 min post-injection of +DOTAP LNPs. CBCs showed that +DOTAP LNPs greatly reduced the number of circulating platelets in mice with pre-existing inflammation (nebulized LPS), and also showed a trend towards reduced platelets in naïve mice (Figure 3a). This reduction in platelet count is dependent on both the number of +DOTAP LNPs injected and the mol fraction of DOTAP in the LNP formulation (Figure S6a,c, Supporting Information). Notably, LNPs targeted to the lung using antibodies against platelet endothelial cell adhesion molecule (PECAM) do not have the same effect on platelets showing that this is due to a positive charge (Figure S9, Supporting Information). Furthermore, ionizable cationic 306-N16B LNPs also significantly decrease platelet count when injected into naïve mice (Figure 3b). Reduced platelet count (thrombocytopenia) can indicate depletion of platelets from circulation due to incorporation in clots. We wanted to investigate if this thrombocytopenia was due to platelet activation by +DOTAP LNPs. To measure platelet activation, we employed flow cytometry. As shown in the schematic of Figure 3c, we used forward scatter (FSC) and side scatter (SSC) measurements to detect larger and more complex platelet aggregates versus small, isolated platelets. We stained for two specific markers of platelets: Glycoprotein V (GPV; CD42d), and P-selectin (CD62p) (Figure S10a,d, Supporting Information). CD42d is constitutively found on the surface of all platelets.^[27] In resting platelets, P-selectin is generally stored in platelet granules, which are externalized when the platelet becomes activated.^[27,28] Platelet-rich plasma (PRP; Figure 3d) was either left untreated or incubated with fluorescently labeled –DOTAP or +DOTAP LNPs and stained for CD42d and P-selectin.

FSC versus SSC plots for platelets (CD42d-positive events) in untreated, –DOTAP, and +DOTAP LNP-treated PRP show

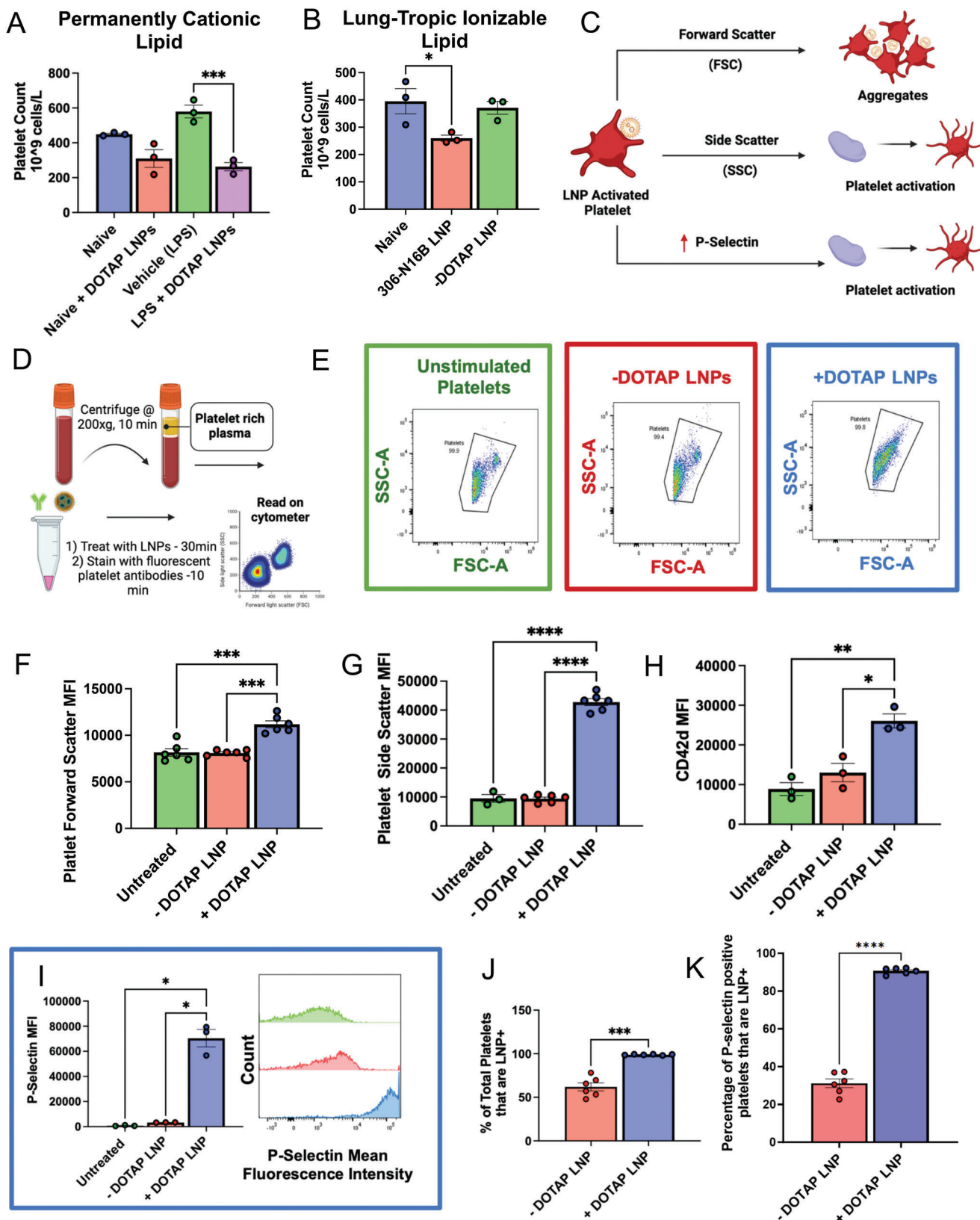
no difference between the untreated and –DOTAP LNP-treated conditions, but the shape of the +DOTAP LNP graph differs markedly from the other two (Figure 3e). The mean FSC and SSC values are elevated for platelets in the presence of +DOTAP LNPs, indicating the formation of aggregates (Figure 3f,g). Further evidence of platelet aggregation induced by +DOTAP LNPs is shown by increased CD42d signal for each CD42d-positive event (Figure 3h). In the presence of +DOTAP LNPs, each CD42d-positive event is a cluster of platelets, rather than an individual cell, so the mean CD42d signal is increased versus untreated and –DOTAP LNP-treated samples. Most interesting, however, is the 20-fold increase in P-selectin presentation induced by +DOTAP LNPs (Figure 3i). Since increased surface presentation of P-selectin is a marker of platelet activation, this demonstrates profound platelet activation induced by +DOTAP LNPs.

Tracing LNP fluorescence in our flow cytometry measurements, we found that 100% of platelets were physically associated with fluorescently labeled +DOTAP LNPs, while only 50% of platelets were physically associated with –DOTAP LNPs, showing that the cationic lipid profoundly increases LNP adhesion to platelets (Figure 3j). Specifically, among platelets that had an LNP signal, we assessed the P-selectin signal. For –DOTAP-LNPs, only 30% of the LNP-associated platelets were P-selectin positive, indicating that –DOTAP LNPs had little effect on platelet activation. However, for +DOTAP LNPs, nearly 100% of LNP-positive platelets were also positive for P-selectin, indicating that platelet association with +DOTAP LNPs predicts platelet activation (Figure 3k).

2.4. DOTAP LNPs bind to Fibrinogen, and Fibrinogen is Required for LNP-Induced Platelet Activation

Having proven that +DOTAP LNPs cause clotting, initiate the coagulation cascade, and activate platelets, we sought to isolate components of the +DOTAP LNP protein corona that might lead to these effects. Upon IV injection, LNPs can form unique protein coronas based on their physicochemical properties and this could alter their functionality.^[29,30] The protein corona can therefore drive the biodistribution and cell-type localization of LNPs. However, the proteins adsorbed on LNPs could also induce side

Figure 2. Coagulation is activated by positively charged LNPs and other nanoparticles, across diverse formulations, both in vivo and in ex vivo whole blood. A) +DOTAP LNPs induce large clots (black arrows) in the pulmonary arteries (scale bar = 100 μm). –DOTAP or +DOTAP LNPs were injected into healthy mice at a dose of 10 μg of mRNA and 30 min after, lungs were harvested and prepared for histology (Masson's trichrome). –DOTAP LNPs do not show such clots. B) In vivo, +DOTAP LNPs increase plasma levels of thrombin-antithrombin (TAT), a marker of recent clotting. The TAT increase is > 2-fold in naïve mice, with an additional > 1.5-fold increase in mice with pre-existing lung inflammation (nebulized-LPS). +DOTAP LNPs were injected into naïve mice and 30 min post-injection, plasma was collected for TAT assay. C) 306-N16B LNPs increase TAT plasma levels by ≈2.5-fold compared to naïve mice while control –DOTAP LNPs do not. 2E11 LNPs per mouse were injected and TAT plasma levels were measured after 30 min. D) Schematic of the two major coagulation pathways – intrinsic and extrinsic – which both converge into the common pathway. The extrinsic pathway is triggered by damage that occurs outside the blood vessel, exposing tissue factors. The intrinsic pathway is initiated by factors within the blood vessel lumen. Both the intrinsic and extrinsic pathways converge to the common pathway which involves the conversion of prothrombin to thrombin – an enzyme that converts fibrinogen to fibrin. Fibrin forms the mesh-like framework of clots. The prothrombin time (PT) and activated partial thromboplastin time (APTT) are laboratory tests used to measure the time to clot through the extrinsic and intrinsic coagulation pathways, respectively. E) +DOTAP LNPs do not change PT time in vitro, showing that they do not induce coagulation through the extrinsic coagulation pathway. F) Timeline and schematic of in vitro APTT measurements. G) +DOTAP LNPs increase APTT, showing that they induce coagulation through the extrinsic pathway. H) +DOTAP LNPs increase APTT through the intrinsic pathway regardless of ionizable lipid identity, as ALC-0315, SM-102, and C12-200 DOTAP LNPs also show elevated APTT. I) Positively charged, non-LNP nanoparticles, here liposomes containing DOTAP, also increase APTT time. Statistics: $n = 3-6$ and the data shown represents mean ± SEM; For (I), comparisons between groups were made using an unpaired *t*-test with Welch's correction. For all other graphs, comparisons between groups were made using one-way ANOVA with Tukey's post-hoc test. * = $p < 0.05$, *** = $p < 0.001$, **** = $p < 0.0001$.



effects. Proteins can undergo conformational changes when adhering to surfaces and aggregates of proteins on surfaces do not often behave similarly to proteins in solution, including causing immunogenic or thrombotic side effects.^[29]

We therefore hypothesized that +DOTAP LNPs could bind to coagulation proteins in plasma, the most abundant being fibrinogen. Fibrinogen is a soluble protein found in plasma. When it is cleaved by thrombin, fibrinogen undergoes conformational changes and aggregates to form fibrin strands, which in turn form the clot-stabilizing mesh. Fibrinogen/fibrin aggregates on surfaces could cause adhesion and activation of platelets. Fibrinogen has a net negative charge at physiological pH and contains domains with a high concentration of negatively charged residues, such as the E domain.^[31,32] Studies have linked the exposure of certain fibrinogen residues to specific side effects.^[33–35] For example, nanoparticle-induced exposure of a peptide sequence at the C-terminus of the fibrinogen γ -chain interacts with the integrin receptor Mac-1 and induces inflammation.^[35] We therefore hypothesized that the positively charged DOTAP in LNPs could interact with, and aggregate fibrinogen in a way that could lead to coagulation and platelet activation. This hypothesis is supported by our finding that +DOTAP LNPs decrease the expression of CD41 on platelets (Figure S10b, Supporting Information). Since CD41 is the platelet receptor of fibrinogen/fibrin, this indicates that there is a blockage of this marker by fibrinogen induced by +DOTAP LNPs.

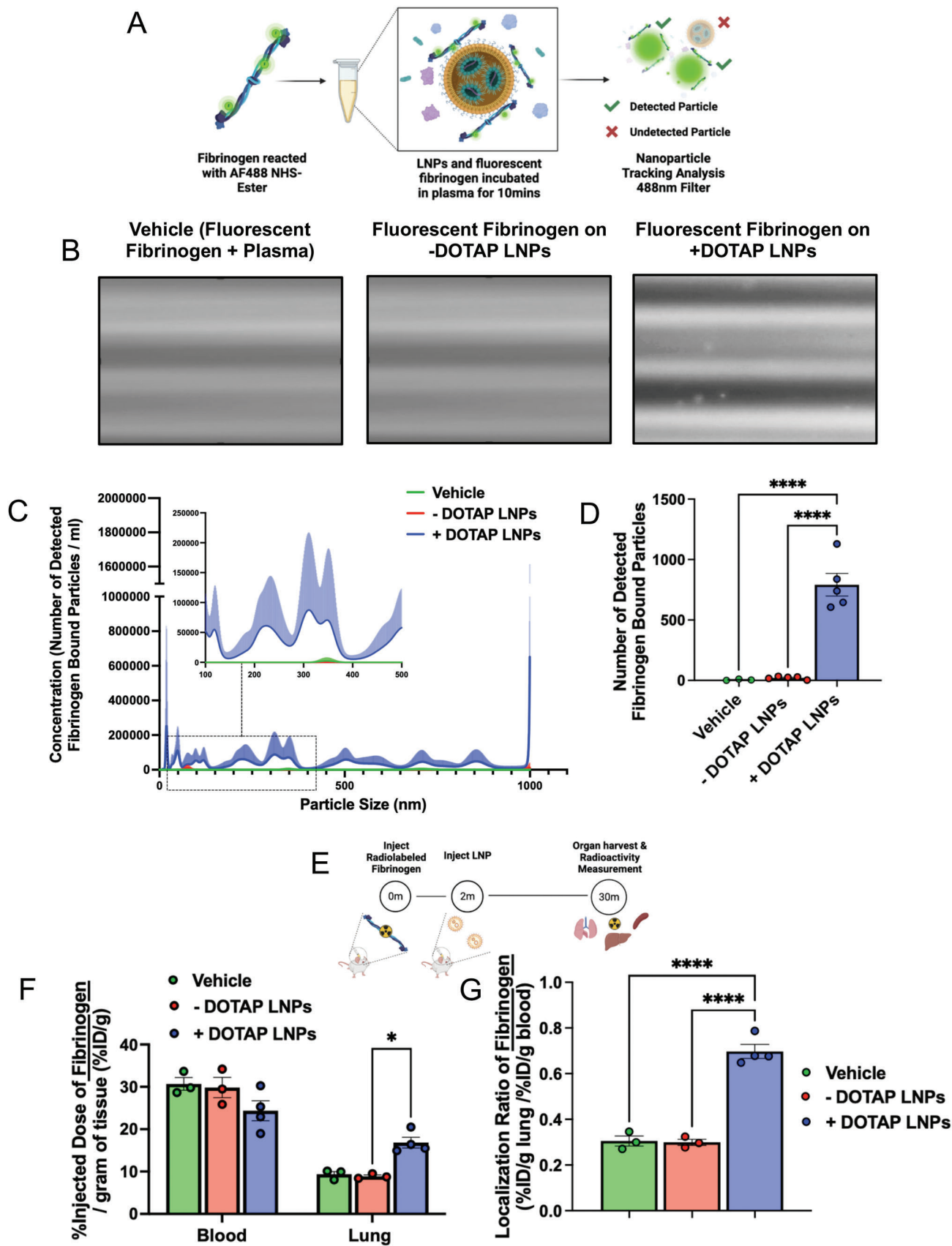
We first tested if +DOTAP LNPs bind to fibrinogen in vitro. We added fluorescently labeled fibrinogen and LNPs to the plasma and incubated for 10 min. We diluted this sample and performed fluorescence-mode nanoparticle tracking analysis (NTA) to detect nanoparticle-sized aggregates of fluorescent fibrinogen, indicating fibrinogen aggregation on LNPs (Figure 4a). Approximately 38-fold more fibrinogen-positive particles were observed in the presence of +DOTAP LNPs versus –DOTAP LNPs (Figure 4b–d). This agrees with our findings that +DOTAP LNPs aggregate significantly with fibrinogen in plasma and even after incubation with fibrinogen alone (Figures S11 and S12, Supporting Information).

We further sought to determine if +DOTAP LNPs bind to fibrinogen in vivo and alter its biodistribution. Fibrinogen was radioactively labeled and injected into mice, followed by + or –DOTAP LNPs 2 min later. Organs were harvested 30 min after LNP injection and the radioactivity in each organ was measured (Figure 4e). While –DOTAP LNPs do not alter fibrinogen biodistribution, there is a \approx 2-fold increase in fibrinogen

lung uptake in the presence of +DOTAP LNPs (Figure 4f,g and Figure S13a, Supporting Information). A similar +DOTAP LNP-induced increase in lung fibrinogen uptake was observed in mice with pre-existing inflammation (Figure S13b, Supporting Information). Notably, the localization of fibrinogen to the lungs induced by +DOTAP LNPs persists even 4 h after injection with evidence of fibrinolysis only 24 h after (Figure S13c–f, Supporting Information). Confocal microscopy images of lung sections show visible aggregates of fibrinogen in +DOTAP LNP-injected mice and no visible fibrinogen in –DOTAP LNP-injected mice (Figure 4h). This was quantified across multiple images, with the LNPs and fibrinogen having much more signal in the lungs of +DOTAP versus –DOTAP LNP mice (Figure 4i). Furthermore, fibrinogen is strongly associated with +DOTAP LNPs as shown by the percentage of fibrinogen signal overlap with that of LNPs or the percentage of LNP signal overlap with fibrinogen signal (Figure 4j). The data in Figure 4a–j show that fibrinogen binds to +DOTAP LNPs (but not –DOTAP LNPs), and this binding correlates with clotting in the lungs. We then performed circular dichroism (CD) to determine if the binding of +DOTAP LNPs to fibrinogen induces changes in the protein's secondary structure. The CD spectra for fibrinogen alone show two negative peaks at 209 and 220 nm which is characteristic of a protein with an α -helix (Figure 4k). However, the addition of +DOTAP LNPs significantly reduces the ellipticity of fibrinogen at both 209 and 220 nm while –DOTAP LNPs do not. This indicates that the secondary structure of fibrinogen is significantly altered in the presence of +DOTAP LNPs which supports the hypothesis that this altered fibrinogen structure could induce platelet activation and coagulation.

To further examine the effects of fibrinogen binding to +DOTAP LNPs, we depleted fibrinogen from plasma doped with +DOTAP LNPs. Since fibrinogen depletion would prevent coagulation, we checked if fibrinogen depletion also abrogated +DOTAP LNP-induced platelet activation. PRP was treated with tissue plasminogen activator (tPA) which converts plasminogen to plasmin, causing degradation of fibrinogen. We found that in fibrinogen-depleted plasma, +DOTAP LNPs do not induce significant platelet activation as measured by P-Selectin MFI (Figure 4l). Thus, fibrinogen is necessary for +DOTAP LNP-induced platelet activation. This fits with a mechanism in which positively charged LNPs first bind to fibrinogen, inducing a conformational change in the protein that activates platelets, which in turn activates the rest of the coagulation cascade. This fits with prior studies that show that immobilization of fibrinogen

Figure 3. DOTAP LNPs cause platelet activation. A) +DOTAP LNPs significantly decrease platelet count in naive mice and even more so in mice with pre-existing inflammation (nebulized LPS). LNPs were IV-injected and platelet count was measured from whole blood 30 min later. B) 306-N16B LNPs decrease platelet count in naive mice while control –DOTAP LNPs do not. C) Schematic depicting what different flow cytometry metrics describe platelet physiology. D) Schematic of protocol used for platelet flow cytometry. After isolation of platelet-rich plasma (PRP), samples were either left untreated or treated with –DOTAP or +DOTAP LNPs for an incubation period of 30 min at 37 °C. E) Representative FSC-A versus SSC-A graphs of unstimulated platelets (green) and platelets treated with +DOTAP (blue) or –DOTAP LNPs (red), showing a clear change in the scatterplot with +DOTAP LNPs. There are significant increases in F) FSC and G) SSC upon treatment with +DOTAP LNPs suggesting larger and more complex platelet aggregates. +DOTAP LNPs cause upregulation of H) CD42d and I) P-selectin, based on mean fluorescence intensity (MFI). J) Platelets were assayed for whether they were physically associated with LNPs, as measured by the fraction of platelets that were positive for a fluorescent lipid that had been incorporated into the LNPs during synthesis. While 50% of platelets were associated with –DOTAP LNPs, nearly 100% of platelets were physically associated with +DOTAP LNPs. K) Staining with P-selectin shows that while only 30% of P-selectin positive platelets were associated with –DOTAP LNPs, almost 100% of P-selectin positive platelets were LNP positive as well, showing preference for an activated state. Statistics: $n = 3–6$ and data shown represents mean \pm SEM; For (J,K), Welch's t -test was performed. For all other graphs, Brown-Forsythe and Welch's ANOVA was performed with the Dunnett T3 post-hoc test. * = $p < 0.05$, *** = $p < 0.001$, **** = $p < 0.0001$.



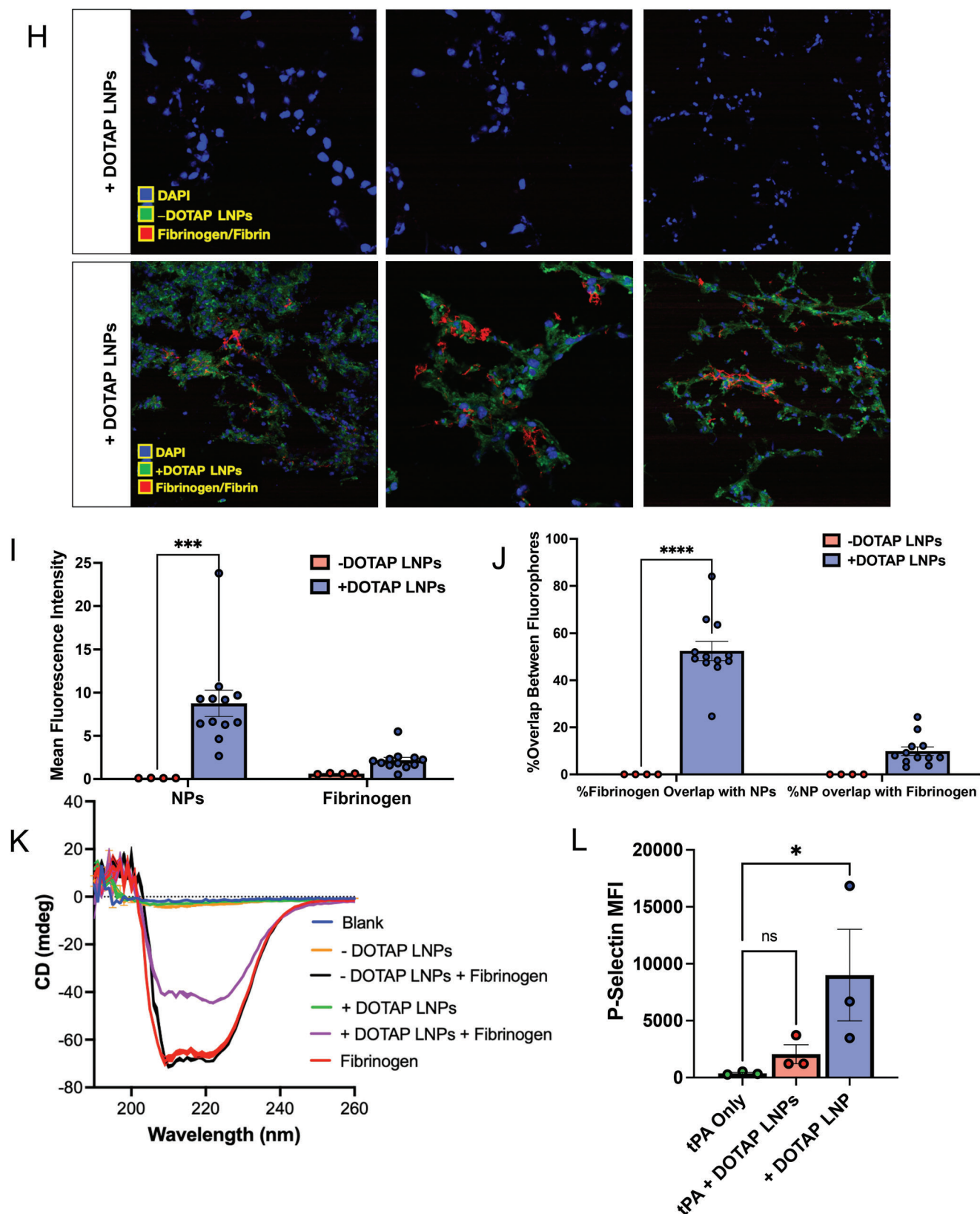


Figure 4. Continued

on surfaces can expose normally concealed domains that activate platelets.^[36–39]

2.5. Anticoagulation Ameliorates Cationic LNP-Induced Clotting

Below, we propose and test ways to prevent LNP-induced clotting. To determine whether anticoagulation can reduce the toxicity of +DOTAP LNPs, we compared clot formation between mice treated with +DOTAP LNPs alone and those pre-treated with the clinically used anticoagulants heparin and bivalirudin. Heparin functions by enhancing the activity of endogenous antithrombin while bivalirudin is a direct thrombin inhibitor. Anticoagulants were IV injected 5 min prior to +DOTAP LNP injection (62.5U per mouse for heparin and 400 µg per mouse for bivalirudin) and LNPs were allowed to circulate for 30 min. We found that both heparin and bivalirudin pre-treatment significantly reduce the formation of clots in the lung compared to +DOTAP LNP injection alone, as shown by lung histological samples (Figure 5a). We then investigated the effect of anticoagulation on +DOTAP LNP biodistribution and mRNA expression. We radiolabeled LNPs with indium-111 for biodistributions and injected mice with LNPs loaded with luciferase mRNA to trace mRNA expression (Figure 5b). Surprisingly, heparin pre-treatment shunted LNP localization from the lung to the liver and spleen and completely attenuated luciferase expression in the lungs (Figure 5c,d, and Figure S14a, Supporting Information). We hypothesize that this unexpected effect is because heparin is a negatively charged polysaccharide, so it could have a charge interaction with +DOTAP LNPs and this could inhibit LNP functionality, though other mechanisms may exist.^[40] By contrast, bivalirudin pre-treatment preserves the localization of +DOTAP LNPs to the lung, as well as the LNP-induced mRNA luciferase expression (Figure 5b,c, and Figure S14b, Supporting Information). These studies illustrate that while the side effects of +DOTAP LNPs can be ameliorated with anticoagulation, the properties of each anticoagulant must be thoroughly examined to ensure that LNP activity is preserved.

Based on this success with bivalirudin (a direct thrombin inhibitor), we tested the effects of a similar anticoagulant, dabigatran (Figure S15, Supporting Information). Furthermore, we fabricated +DOTAP LNPs with a surface-conjugated direct thrombin inhibitor, PPACK (Figure S16, Supporting Information).^[41] This might be a more convenient clinical solution than needing to transiently anticoagulate patients with bivalirudin. Clot formation in the lungs was also limited in mice treated with PPACK-conjugated +DOTAP LNPs (Figure S16d, Supporting Information).

2.6. Decreasing the Size of DOTAP LNPs Prevents Fibrinogen Binding and Clotting

We serendipitously observed that the size of +DOTAP LNPs has a positive correlation with APTT. When we increased LNP size from 100 nm to 180 nm, APTT increased by ~1.6-fold. However, when we decreased the LNP size to 80 nm, APTT was restored to naive levels indicating no significant activation of the intrinsic coagulation pathway (Figure 6a). Similarly, 80 nm +DOTAP LNPs did not significantly activate platelets, as measured by P-selectin MFI (Figure 6b). This led us to hypothesize that the size of +DOTAP LNPs could affect the amount of fibrinogen molecules that can be adsorbed on the LNP surface. We tested this hypothesis first in vitro using fluorescence NTA to probe for fibrinogen aggregation and found that 80 nm +DOTAP LNPs generate ~79× fewer nanoparticle-associated fibrinogen aggregates than 100 nm +DOTAP LNPs (Figure 6c,d). Additionally, the number of fibrinogen-nanoparticle aggregates detected with 80 nm +DOTAP LNPs is not significantly different from that under vehicle conditions, indicating a complete absence of detectable fibrinogen-nanoparticle aggregation. We subsequently tested how 80 nm +DOTAP LNPs affect fibrinogen biodistributions in vivo. As previously, we injected mice with radiolabeled fibrinogen followed by LNPs 2 min after for a circulation time of 30 min. While 100 nm +DOTAP LNPs almost double fibrinogen uptake in the lung, 80 nm +DOTAP LNPs do not alter

Figure 4. Fibrinogen binds to +DOTAP LNPs, is required for LNP-induced activation of platelets, and is likely the first step in LNP-induced clotting. A) To measure LNP binding to fibrinogen, we fluorescently labeled fibrinogen, mixed it with plasma and LNPs, and used nanoparticle tracking analysis (NTA) to identify individual nanoparticles that had become bound to fluorescent fibrinogen. B) Representative NTA images of fluorescent fibrinogen on –DOTAP or +DOTAP LNPs, showing visible binding of fibrinogen to +DOTAP LNPs but no visible binding to –DOTAP LNPs, or vehicle control. C) NTA data was turned into particle size versus concentration histograms, and here we plot fibrinogen-positive particles only. +DOTAP LNPs bind strongly to fluorescent fibrinogen and this leads to LNPs of many different sizes, while –DOTAP LNPs barely have any fibrinogen-positive signal at any particle size. Inset: Size versus concentration histogram ranging from 100–500 nm. D) Number of detected fibrinogen-bound particles from (C) showing that +DOTAP LNPs generate ~37.7× more fibrinogen-bound particles than –DOTAP LNPs. E) Next, we IV-injected radiolabeled fibrinogen into mice, followed by LNPs 2 min later. Organs were harvested 30 min after LNP injection and the radioactivity in each organ was measured. F) Amount of radiolabeled fibrinogen in the blood and lungs after the protocol of (E), shown as the % of injected dose per gram of tissue (%ID g⁻¹). +DOTAP LNPs lead to a ~2× increase in fibrinogen lung uptake, while –DOTAP LNPs do not alter fibrinogen biodistribution compared to control. G) Localization ratios of fibrinogen from (F) calculated as %ID g⁻¹ of tissue in the lung divided by that in the blood. +DOTAP LNPs cause a 2.4-fold higher localization ratio of fibrinogen compared to –DOTAP LNPs and vehicles. H) Representative confocal microscopy images of lung sections from mice injected with fluorescent fibrinogen followed by fluorescent LNPs, showing visible fibrinogen aggregates in the lungs of +DOTAP LNP injected mice (*n* = 3 biologically independent animals). I) Mean fluorescence intensities (MFIs) in the lung sections from (H) of – or +DOTAP LNPs and fibrinogen showing significantly higher MFIs of LNPs and fibrinogen in +DOTAP LNP injected mice compared to –DOTAP LNP mice. J) From the microscopy images in (H), the percentage of fibrinogen signal overlap with that of LNPs or percentage of LNP signal overlap with fibrinogen signal in the presence of – or +DOTAP LNPs shows a strong co-localization of fibrinogen with +DOTAP LNPs. K) Circular dichroism of fibrinogen (1 mg ml⁻¹) in the presence of –DOTAP or +DOTAP LNPs (4E11 LNPs per ml) reveals that +DOTAP LNPs alter the secondary structure of fibrinogen while –DOTAP LNPs do not. L) To determine if fibrinogen is necessary for LNP-induced activation of platelets, we added tPA to plasma to deplete the fibrinogen. Fibrinogen depletion nearly completely prevented LNP-induced activation of platelets. Statistics: *n* = 4–12 for (I) and (J) and *n* = 3–4 for all other graphs. Data shown represents mean ± SEM; For (F), (I), and (J), comparisons between groups were made using two-way ANOVA with Tukey's post-hoc test. For all other graphs, comparisons between groups were made using one-way ANOVA with Tukey's post-hoc test. * = *p* < 0.05, *** = *p* < 0.001, **** = *p* < 0.0001.

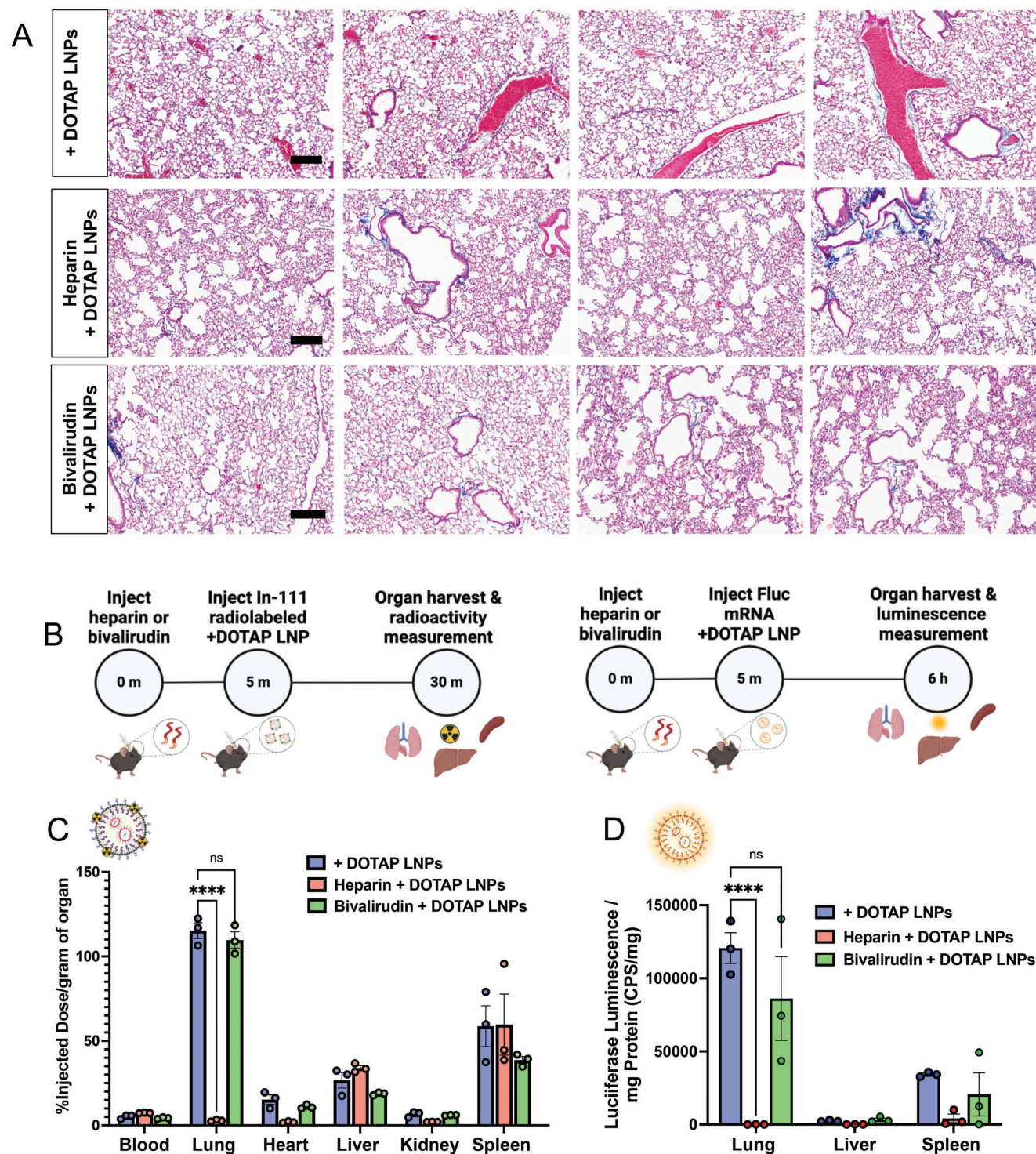
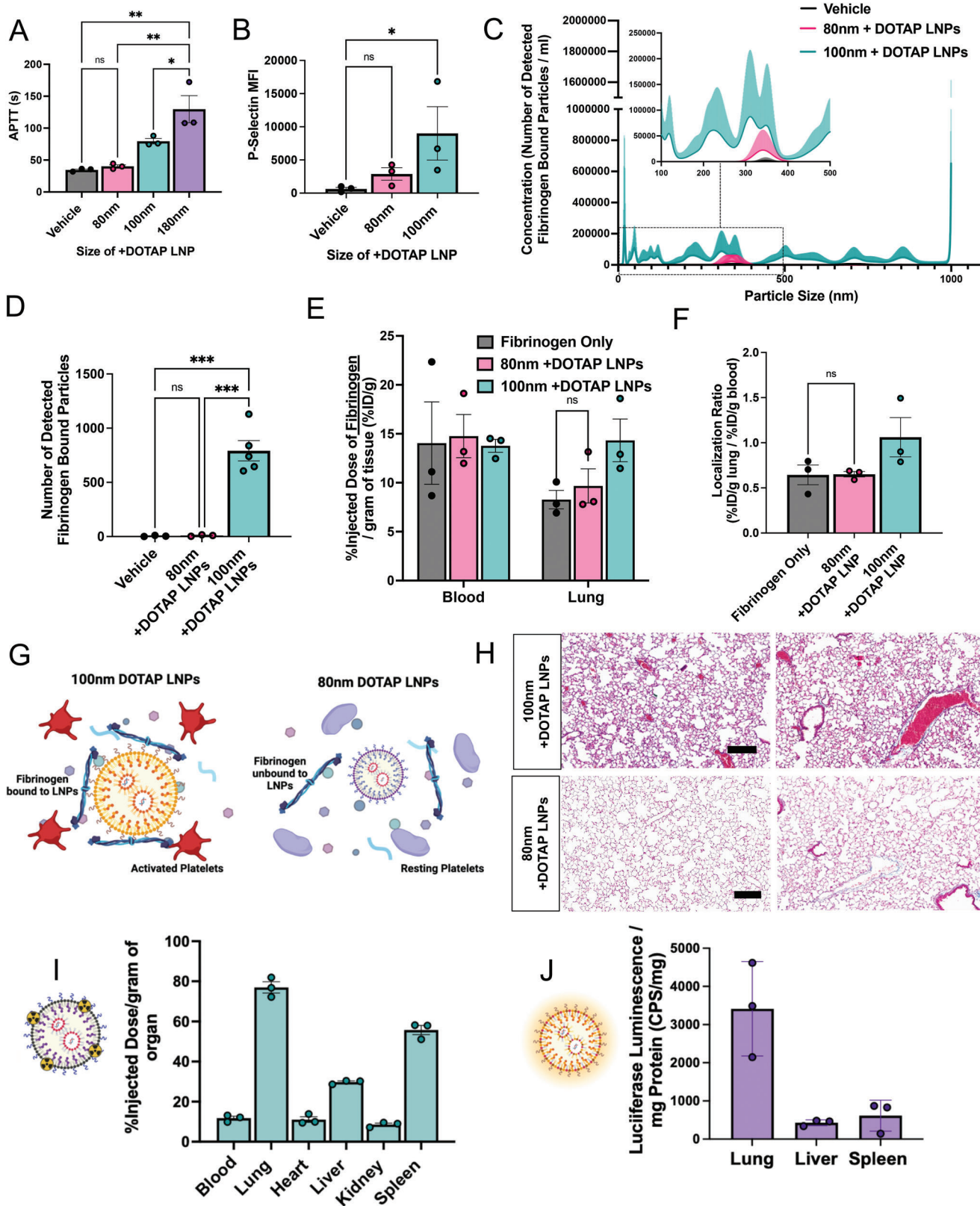


Figure 5. Anticoagulation ameliorates the side effects of DOTAP LNPs, but only select anticoagulants still allow LNP targeting to the lungs. A) Histology showing clots in the lungs of mice given +DOTAP LNPs (top row), but not in mice that were given +DOTAP LNPs preceded by heparin (middle row) or bivalirudin (bottom row; scale bar = 200 μ m). B) Schematics showing the protocol for biodistribution studies (using In-111-labeled LNPs) and luciferase expression studies. C) 30-min biodistribution in naïve mice of +DOTAP LNPs with no treatment or pretreated with heparin or bivalirudin. Pretreatment with heparin ablates localization of +DOTAP LNPs to the lung. Interestingly, pretreatment with bivalirudin maintains lung localization. D) Additionally, bivalirudin further preserves luciferase expression of +DOTAP LNPs whereas heparin pretreatment attenuates this expression capacity. Statistics: $n = 3$ and the data shown represents mean \pm SEM. For (C) and (D), comparisons between groups were made using a two-way ANOVA with Tukey's post-hoc test. * = $p < 0.05$, *** = $p < 0.001$, **** = $p < 0.0001$.



fibrinogen biodistribution or localization ratio compared to control (Figure 6e,f). These data validate our hypothesis that 80 nm +DOTAP LNPs do not detectably bind to or cause aggregation of fibrinogen. Since this interaction is associated with thrombosis, these LNPs do not activate platelets or the intrinsic coagulation pathway (Figure 6g). Furthermore, histological samples from the lungs of LNP-injected mice show that 80 nm +DOTAP LNPs do not generate visible clots like 100 nm +DOTAP LNPs (Figure 6h). Finally, 80 nm +DOTAP LNPs still preserve their lung tropism, as shown by their biodistribution and mRNA expression profile (30-min and 4-h LNP circulation time respectively) (Figure 6i,j). These data indicate that by altering the physical properties of +DOTAP LNPs, we can modulate the binding of fibrinogen and the subsequent initiation of clotting while maintaining lung tropism.

3. Discussion

Nanoparticles are prone to attack by blood's defense systems. Two of the major defense systems of blood, complement proteins and immunoglobulins, have been repeatedly shown to attack nanoparticles. But a third blood defense, clotting, is often overlooked by the field of nanomedicine, especially the booming field of LNPs, as this is the first report of LNP-induced thrombosis. Since intravascular clotting leads to potentially deadly, acute thrombosis, investigation of clotting side effects should be a standard part of IV nanomedicine development. There have been prior studies showing thrombotic side effects of other types of nanoparticles, but these studies have been largely neglected with the most clinically important nanomedicines today: LNPs. As the field of nanomedicine rapidly moves towards using charged lipids and other physicochemically less defined mechanisms as a primary tool for targeting, studies of clotting responses to nanomedicines, especially LNPs, are critically timely and necessary.

Among the reasons that the LNP field had not previously observed clotting, a major one is likely the methods used for testing LNPs in vitro. In vitro studies of blood responses to nanoparticles often use serum, rather than plasma. Plasma is the acellular component of blood. Serum is prepared by depleting clotting factors from plasma, so it is impossible to

study clotting responses with serum. For instance, fibrinogen, critical to side effects observed in our studies, is missing from serum. Even in studies of plasma, one misses the critical role of platelets, shown here to serve as a pro-thrombotic surface that is activated by and amplifies the pro-coagulant effects of cationic LNPs. Nanomedicine's focus on complement as a central source of side effects may also miss upstream coagulation side effects: Thrombin and plasmin activate the complement cascade. In vitro and in vivo studies that assessed nanoparticle interactions with the acellular and cellular components of blood involved in clotting were necessary to evaluate the deadly side effects identified here, and similar studies may be called for in developing other physicochemical targeting approaches.

Here we have focused on clotting associated with LNPs that bear a positive zeta potential, but future studies will need to investigate other nanoparticle properties that induce clotting. In this current study, we showed that clotting is induced by lung-tropic LNPs containing either permanently cationic lipids (possessing quaternary amines), or even those containing only an ionizable lipid (possessing only tertiary amines) whose charge dynamics are such that the overall LNP zeta potential is positive. These effects held across a wide range of LNP lipid constituents (varying ionizable lipids, charged lipids, etc). This strongly implicates the presence of positive zeta potential as a nanoparticle feature that increases thrombosis risk. But we also identified a nanoparticle feature that reduces thrombosis risk: varying nanoparticle size had a large effect on clot induction, with a size below ≈ 100 nm limiting thrombosis induced by +DOTAP LNPs in mice. Many additional nanoparticle properties must be tested for their relationship to clotting, including mechanical properties (Young's modulus, surface fluidity), polymeric brush borders (e.g., PEG), and appended proteins (e.g., antibodies used to target LNPs to specific epitopes). Such a systematic survey, coupled with biophysics studies of nanoparticle binding to coagulation proteins, will enable the design of safer nanoparticles.

Just as nanoparticle properties must be studied in relation to clotting, we must also investigate how changes in the blood itself might affect nanoparticle-associated clotting. While these studies were done in mice, we must now assay for nanoparticle-associated clotting in human blood, as well as the large animals commonly used in preclinical efficacy and toxicity studies (pig, sheep, and non-human primates), noting that small animal

Figure 6. Decreasing the size of DOTAP LNPs prevents fibrinogen binding and the resulting coagulation and platelet activation. A) +DOTAP LNP size has a positive correlation with coagulation as measured by APTT. 180 nm +DOTAP LNPs lead to a ≈ 1.6 -fold increase in APTT compared to standard 100 nm +DOTAP LNPs while 80 nm +DOTAP LNPs maintain APTT at naive levels. B) 80 nm +DOTAP LNPs do not cause significant platelet activation as measured by P-Selectin MFI. C) Particle size versus concentration histograms from the NTA fluorescent fibrinogen binding assay comparing the number of detected fibrinogen bound particles with 80 or 100 nm +DOTAP LNPs showing that 80 nm +DOTAP LNPs bind to significantly less fibrinogen compared to 100 nm +DOTAP LNPs. Inset: Size versus concentration histogram ranging from 100–500 nm. D) Number of detected fibrinogen-bound particles from (C) showing that 80 nm +DOTAP LNPs generate $\approx 79\times$ fewer fibrinogen-bound particles than 100 nm +DOTAP LNPs. The number of fibrinogen-bound particles detected with 80 nm +DOTAP LNPs is not significantly different from the vehicle. E) Amount of fibrinogen in the blood and lungs with injection of radiolabeled fibrinogen alone (vehicle) or radiolabeled fibrinogen followed by 80 or 100 nm +DOTAP LNPs. 80 nm +DOTAP LNPs do not alter fibrinogen biodistribution compared to control. F) 80 nm +DOTAP LNPs do not alter the localization ratio of fibrinogen calculated from (E) ($\%ID\ g^{-1}$ of tissue in the lung divided by that in the blood). G) Hypothesized mechanism behind the abrogation of clotting side effects below a size threshold: At a large radius of curvature (≥ 100 nm), +DOTAP LNPs present a flat enough surface to bind fibrinogen lengthwise, which then activates platelets. H) Lung histological samples reveal that 80 nm +DOTAP LNPs do not generate visible clots as is the case with 100 nm +DOTAP LNPs. I) 80 nm +DOTAP LNPs maintain their biodistribution and lung localization (10 μg mRNA per mouse, 30 min; scale bar = 200 μm) and J) express mRNA primarily in the lung measured by luciferase expression (10 μg mRNA per mouse, 4 h). Statistics: $n = 3$ and the data shown represents mean \pm SEM. For (E), comparisons between groups were made using a two-way ANOVA with Tukey's post-hoc test. For all other graphs, comparisons between groups were made using one-way ANOVA with Tukey's post-hoc test. * = $p < 0.05$, *** = $p < 0.001$, **** = $p < 0.0001$.

models often do not capture fatal embolic side effects that emerge in larger animals and humans. We should also investigate how various disease states and medications that affect the blood might predispose or protect from nanoparticle-associated clotting. Here we showed that pre-existing inflammation worsens the magnitude of LNP-induced lung injury, but more in-depth mechanistic studies are required, as well as testing in other relevant disease states, such as common procoagulant genotypes (factor V Leiden, proteins C & S deficiency), cancers with clotting predispositions (noting that clotting is associated with metastasis), and other inflammatory diseases. Indeed, fibrinogen is an “acute phase reactant,” meaning that its concentration in plasma goes up dramatically during inflammation (and many cancers), thus making it more likely to bind to LNPs. These studies in different disease states are essential, because many of the proposed applications of LNPs are for cancer and inflammatory diseases, and thus nanoparticle-induced clotting could become more prominent and dangerous, perhaps occurring even for smaller LNPs or LNPs without positively charged lipids.

While studying LNPs in the above thrombophilic states, it will be essential to further optimize the clot prevention techniques used with any LNPs that possess a positive zeta potential. Here we showed improvement with three anti-thrombosis methods (systemic anticoagulation, conjugating thrombin inhibitors to LNPs, and smaller LNP diameter) in mice, but it is likely these techniques will have to be either combined or extended to be safe in human thrombophilic states. Thus, additional work is necessary to make positive-zeta-potential LNPs truly safe for clinical use.

Finally, more mechanistic studies are needed to further understand nanoparticle-induced clotting. Here we showed that fibrinogen binds to positively charged LNPs (Figure 4b–j) and it is likely that this is due to an electrostatic interaction between these LNPs and the negatively charged domains of fibrinogen such as the D and E domains, similar to other charged particles.^[33,42] We have shown that this binding leads to a large change in the conformational change of fibrinogen (Figure 4k). We therefore hypothesize that fibrinogen binding to LNPs changes its conformation to resemble its activated form. Such surface-bound fibrinogen/fibrin is known to bind to GPIIB/IIIA on platelets, immobilizing and leading to activation of the platelets. Indeed, we showed that fibrinogen-binding +DOTAP LNPs induce platelet aggregation and activation (Figure 3) and that depletion of fibrinogen abrogates +DOTAP LNP-induced platelet activation (Figure 4l). But many mechanistic questions remain, such as why fibrinogen binding is so sensitive to the LNP radius of curvature, and whether clinically used platelet inhibitors (aspirin, clopidogrel, and especially the GPIIB/IIIA inhibitor tirofiban) would prevent LNP-induced clotting. Such future mechanistic studies will likely improve our techniques to prevent LNP-associated clotting and could make physicochemical targeting of LNPs safer and more effective.

4. Experimental Section

Materials: DOTAP, 1,2-dioleoyl-snglycero-3-phosphoethanolamine (DOPE), cholesterol, 1,2-dimyristoyl-rac-glycero-3-methoxypolyethylene glycol-2000 (DMG-PEG 2000), dipalmitoyl phosphatidylcholine (DPPC), 1,2-dioleoyl-sn-glycero-3-phosphoethanolamine-N-(TopFluor AF594) (18:1 PE TopFluor AF 594, ammonium salt), 1,2-distearoyl-sn-

glycero-3-phosphoethanolamine-N-diethylenetriaminepentaacetic acid (18:0 PE-DTPA, ammonium salt), 1,2-dioleoyl-sn-glycero-3-phospho-L-serine (DOPS, sodium salt), and 1,2-distearoyl-sn-glycero-3-phosphoethanolamine-N-[azido(polyethylene glycol)-2000] (DSPE-PEG2000-azide, ammonium salt) were purchased from Avanti Polar Lipids.

Ionizable lipids cKK-E12, 306-N16B, SM-102, ALC-0315, and C12-200 were purchased from Echelon Biosciences. Anti-mouse BV421 CD41, PE-Cy7 CD62P AF700 Ly6G, and APC CD42d were purchased from Biolegend. Indium-111 chloride (In-111) was purchased from BWXT Medical. A modified Lowry assay kit (DC Protein Assay) was purchased from Bio-Rad Laboratories. tPA was purchased from Millipore.

Animals: All animal studies were carried out in accordance with the Guide for the Care and Use of Laboratory Animals (National Institutes of Health, Bethesda, MD), and all animal protocols were approved by the University of Pennsylvania Institutional Animal Care and Use Committee. All animal experiments were carried out using male, 6–8 week old C57BL/6 mice (23–25 g) (The Jackson Laboratory, Bar Harbor, ME). The mice were maintained at 22–26 °C and adhered to a 12/12 h dark/light cycle with food and water ad libitum. For all experiments, mice were anesthetized in a chamber with 4% isoflurane in 100% oxygen.

Nanoparticle Formulation: LNPs were formulated using the microfluidic mixing method. An organic phase containing a mixture of lipids dissolved in ethanol at a designated molar ratio (Table S1, Supporting Information) was mixed with an aqueous phase (50 mM citrate buffer, pH 4) containing luciferase mRNA that was either purchased by TriLink (most experiments) or made in-house via in vitro transcription (IVT)^[43] at a flow rate ratio of 1:3 and at a total lipid/mRNA weight ratio of 40:1 in a microfluidic mixing device (NanoAssemblr Ignite, Precision Nanosystems). LNPs were dialyzed against 1 × PBS in a 10 kDa molecular weight cut-off cassette for 2 h, sterilized through a 0.22 μm filter, and stored at 4 °C.

To manufacture LNPs of 180 nm, the flow rate of the NanoAssemblr Ignite varied, from 6 mL min⁻¹ (for 100 nm) to 1 mL min⁻¹ (180 nm). The authors were unable to produce uniform LNPs < 100 nm with TriLink mRNA, but with in-house IVT mRNA, LNPs of 80 nm were made at a flow rate of 6 mL min⁻¹.

Liposomes were synthesized using the thin film hydration method. Lipids were dissolved in chloroform and combined in a borosilicate glass tube. Chloroform and ethanol were evaporated by blowing nitrogen over the solution until visibly dry (≈15 min) and then placed in the tube under vacuum for > 1 h. Dried lipid films were hydrated with 1 × PBS, pH 7.4 to a total lipid concentration of 20 mM. The rehydrated lipid solution was vortexed and sonicated in a bath sonicator until visually homogeneous (≈1 min each of vortexing and sonication). The solution was then extruded 21 times through a 0.2 μm polycarbonate filter.

Nanoparticle Characterization: Dynamic light scattering measurements of hydrodynamic nanoparticle size, distribution, polydispersity index, and zeta potential were made using a Zetasizer Pro ZS (Malvern Panalytical). LNP RNA encapsulation efficiencies and concentrations were measured using a Quant-iT RiboGreen RNA assay (Invitrogen).

Nebulized LPS Model: Mice were exposed to nebulized LPS in a “whole-body” exposure chamber, with separate compartments for each mouse (MPC-3 AERO; Braintree Scientific, Inc.; Braintree MA). To maintain adequate hydration, mice were injected with 1 mL of sterile saline, 37 °C, intraperitoneally, immediately before exposure to LPS. LPS (L2630-100 mg, Sigma Aldrich) was reconstituted in PBS to 10 mg mL⁻¹ and stored at -80 °C until use. Immediately before nebulization, LPS was thawed and diluted to 5 mg mL⁻¹ with PBS. LPS was aerosolized via a mesh nebulizer (Aerogen, Kent Scientific) connected to the exposure chamber (NEB-MED H, Braintree Scientific, Inc.). 5 mL of 5 mg mL⁻¹ LPS was used to induce the injury. Nebulization was performed until all liquid was nebulized (≈20 min).

TAT and Blood Count Measurements: LNPs were retro-orbitally injected into naïve or nebulized LPS-injured mice for a circulation time of 30 min. Blood was collected from mice into tubes containing EDTA. Blood cells were analyzed using an Abaxis VetScan HM5 Hematology Analyzer for complete blood counts. Blood was then centrifuged at 1500 × g for 10 min

and plasma was collected and analyzed with a TAT ELISA kit (Abcam) according to the manufacturer's instructions.

Lung Histology: LNPs were retro-orbitally injected into naïve mice for a circulation time of 30 min. After exsanguination and perfusion via the right ventricle with ≈ 5 mL of phosphate-buffered saline (PBS) at a constant pressure of 25 cm H₂O, whole lungs were inflated and fixed with neutral buffered 10% formalin. Paraffin-embedded 5 μ m lung sections were stained and imaged with Masson's trichrome by the Pathology Core Laboratory of Children's Hospital of Philadelphia.

In Vitro and In Vivo PT, APTT, and Time to Clot Assays: PT and APTT measurements were carried out with a SStart Analyzer (Stago) and Pacific Hemostasis reagents at a temperature of 37 °C. In these studies, an oscillating stainless steel ball was placed in the sample and after the formation of a clot, this ball was attenuated and the time interval for clot formation was automatically recorded. Blood was first collected from naïve mice and anticoagulated with 3.2% sodium citrate at a ratio of 10:1, blood:citrate, vol:vol. Blood samples were then centrifuged at 1500 \times g for 10 min and the plasma was collected. 50 μ l of plasma was incubated with 0.5 μ g of mRNA in LNPs or a specified number of particles for 5 min. For the PT assay, 50 μ l of LNP-treated plasma was diluted up to 100 μ l with PBS and 200 μ l of PT reagent (Pacific Hemostasis) was added and the time to clot was automatically measured. For the APTT assay, 50 μ l of LNP-treated plasma was diluted up to 100 μ l of PBS and 100 μ l of APTT-XL reagent (Pacific Hemostasis) was added for an incubation time of 4 min. 100 μ l of 0.02 M calcium chloride was then added and the time to clot was automatically measured. For in vivo measurements, blood was collected from treated mice and then centrifuged at 1500 \times g for 10 min to isolate the plasma. Plasma was then analyzed as described.

For time-to-clot assays, 50 μ l of plasma was placed in the SStart Analyzer with an oscillating stainless steel ball. After recalcification with 100 μ l of 0.02 M calcium chloride, the time to clot was immediately measured based on the attenuation of the ball.

NTA Assay for Fibrinogen Aggregation with LNPs: To prepare fluorophore-labeled fibrinogen, mouse fibrinogen (Innovative Research) was incubated with NHS ester Alexa Fluor 488 (ThermoFisher) at 1:10 mol:mol ratio in PBS at 4 °C for 16 h. Afterward, excess fluorophore was removed from fibrinogen by a 3-fold passage against a 10 kDa molecular weight cut-off centrifugal filter (Amicon) with PBS washing between passages. After fibrinogen recovery from the centrifugal filter, spectrophotometer measurement of optical density at 280 nm (Nanodrop) determined fluorescent fibrinogen concentration and optical density measurement at 488 nm determined the number of fluorophores per fibrinogen.

Immediately before experiments, LNP concentrations were determined by NTA (Nanosight, Malvern). In a total reaction volume of 40 μ l, 4E10 LNPs were combined with 20 μ l of heparinized mouse serum (a pooled sample obtained from $n = 3$ mice) and fluorescent fibrinogen was doped into the solution at a final physiologically relevant concentration of 3 mg mL⁻¹. Fluorescent fibrinogen, serum, and LNPs were incubated in the dark at room temperature for 10 min. Fluorescent fibrinogen was also added to serum solutions at identical concentrations, without LNPs, verifying that fluorescent fibrinogen did not detectably adhere to endogenous serum components. The fibrinogen-serum-LNP reactions were terminated by 1:250 dilution in PBS and the diluted suspensions were used for nanoparticle tracking analysis. NTA was conducted with a 488 nm excitation laser and a 500 nm long pass filter to image and track the Alexa Fluor 488 signal from fluorescent fibrinogen on LNPs. Automated analysis of fluorescence nanoparticle tracking data in Malvern Nanosight software used a uniform detection threshold of 5 for all samples. For both fluorescence data and scattering data, three to five technical replicates were obtained for each sample and an average of those replicates was taken as representative of the size-concentration profile for each sample.

Circular Dichroism: Measurements were recorded using a 1500 circular dichroism spectrometer (Jasco) with a 1 mm path length quartz cell over a wavelength range of 190–260 nm. Data were collected at a temperature of 37 °C with a bandwidth of 1 nm at 50 nm min⁻¹ and a CD scale of 200mdeg/0.1dOD. Fibrinogen was diluted in PBS at a concentration of

1 mg mL⁻¹ and for readings with LNPs, 4E11 particles were incubated with fibrinogen for 5 min before reading.

Radiolabeling and Biodistributions: For biodistribution studies, nanoparticles were traced with In-111 as previously described.^[44] Nanoparticles were produced as described above with 0.1 mol% of 18:0 PE-DTPA (a chelator containing lipid) using metal-free buffers. Trace metals were removed from the buffers using a Chelex 100 resin, per the manufacturer's instructions, to prevent unwanted occupancy of the chelator. In-111 chloride was added to the nanocarriers at a specific activity of 1 μ Ci of In-111 per 1 μ mol of lipid. The mixture was incubated at room temperature for 30 min. Then, unincorporated In-111 was removed using a Zeba Spin desalting column. The removal of unincorporated In-111 was verified using thin film chromatography (TLC). A 1 μ l sample of nanoparticles was applied to the stationary phase (silica gel strip). The strip was placed in the mobile phase of 10 mM EDTA until the solvent front was 1 cm from the end of the strip (≈ 10 min). The strip was cut 1 cm above the initial sample location. In-111 chelated to the nanoparticles stayed at the origin, while unchelated In-111 traveled with the solvent front. The activity in each section was measured using a gamma counter. The percent of In-111 chelated to the nanoparticles was calculated as the activity in the origin strip divided by the total activity in both strips. For all experiments, > 95% of In-111 was chelated to the nanoparticles.

For biodistributions of fibrinogen, the protein was radiolabeled with iodine-125 using the Iodogen method. Tubes coated with 100 μ g of Iodogen reagent were incubated with fibrinogen (2 mg mL⁻¹) and Na¹²⁵I (115 μ Ci per μ g protein) for 5 min on ice. Unincorporated I-125 was removed with a Zeba column followed by TLC analysis as described above.

For nanoparticle biodistributions, In-111 labeled nanoparticles were injected into mice for a circulation time of 30 min. For fibrinogen biodistributions, I-125 fibrinogen was allowed to circulate for 2 min before the injection of nanoparticles for 30 min before harvest. The radioactivity in each organ was then read with a gamma counter (Wizard2, PerkinElmer).

Confocal Microscopy: Healthy mice were injected with 150 μ g of fibrinogen fluorescently labeled with AF647-NHS-Ester. Two minutes later, mice were injected with fluorescent + or -DOTAP LNPs formulated with 0.3 mol % of 18:1 PE TopFluor AF 594. After a 30-min circulation the animals were sacrificed and perfused with 5 ml of cold PBS and lungs were harvested and freshly frozen. 10 μ m lung slices were cryosectioned for imaging using a Leica TCS SP8 confocal microscope.

Luciferase Delivery: Luciferase mRNA LNPs fabricated as described above were injected into mice for a circulation time of 4 h. Select organs were then flash-frozen until the day of analysis or homogenized immediately. Samples were suspended in 900 μ l of homogenization buffer (5 mM EDTA, 10 mM EDTA, 1:100 diluted stock protease inhibitor [Sigma], and 1 \times PBS, samples were then loaded with a steel bead [Qiagen], then placed in a tissue homogenizer [Powerlyzer 24, Qiagen] using the following settings: Speed (S) 2000 rpm, 2 cycles (C), time (T) 45 s, and pause for 30 s). After this, 100 μ l of lysis buffer (10% Triton-X 100 and PBS) was added into each tube and then allowed to incubate for 1 h at 4 °C. After this, they were immediately transferred into fresh tubes, and sonicated, using a point sonicator to remove in excess DNA, using an amplitude of 30%, five cycles of 3 s on/off. After this, samples were then centrifuged at 16 000 \times g for 10 min. The resultant lysate was either frozen or prepared for luminometry analysis. For luciferase expression, 20 μ l of undiluted sample was loaded onto a black 96 well-plate and then 100 μ l luciferin solution (Promega) was added immediately before reading on a luminometer (Wallac). Last, a Lowry assay (Bio-Rad) was performed according to manufacturer's specifications using diluted samples, specifically a 1:40 dilution for lung and spleen tissues and a 1:80 dilution for liver tissues. Final luminescence readings were then normalized based on the total protein concentration obtained from the Lowry assay.

Platelet Flow Cytometry: Platelet-rich plasma (PRP) was collected by first adding 15 μ l of 10 mg mL⁻¹ bivalirudin as well as flushing 23G collection needles with the same solution bivalirudin, collecting between 500–1000 μ l of blood per mouse. After the blood draw, samples were then centrifuged at room temperature (RT) at 200 \times g for 10 min. After centrifugation, PRP was collected, taking care not to disturb the resultant pellet. After collection, samples were immediately read on a hematology

analyzer (Vetscan HM2, Abaxis) to obtain platelet count. Resultant platelets were then aliquoted to achieve a total of 400 000 platelets per analysis with Tyrode's buffer. These platelet samples were then incubated with 0.5 µg mRNA dose of AlexFluor 594 labeled –DOTAP or +DOTAP LNPs for 30 min at 37 °C. After incubation with nanoparticles, samples were stained with flow cytometry antibodies against CD41, CD42d, and P-selectin and allowed to incubate at RT for 10 min. Samples were then immediately diluted with 350 µL of Tyrode's buffer and read on LSR Fortessa (BD Bioscience). Analysis was then completed using FloJo and the gating strategy employed is found in Figure S8, Supporting Information. For fibrinogen-depleted plasma, 0.278 mg of tPA was added per mL of platelet-free plasma, followed by 3 h incubation at 37 °C.

Statistics: All results were expressed as mean ± SEM unless specified otherwise. Statistical analyses were performed using GraphPad Prism 8 (GraphPad Software) * denotes $p < 0.05$, ** denotes $p < 0.01$, *** denotes $p < 0.001$, **** denotes $p < 0.0001$.

Supporting Information

Supporting Information is available from the Wiley Online Library or from the author.

Acknowledgements

S.O.-L. and M.E.Z. contributed equally to this work. Research reported in this publication was supported by the American Heart Association under Grant 23PRE1014444 (to S.O.-L.), Ruth L. Kirschstein National Research Service Award (NRSA) F31HL154662 (to M.E.Z.) American Heart Association under Grant 916172 (to J.N.), PhRMA Foundation under grant 2023 PFDL 1008128 (to Z.W.), and Grant NIH R01 HL157189 (to V.M., J.W.M., and J.S.B.). The data for this manuscript were generated in the Penn Cytomics and Cell Sorting Shared Resource Laboratory at the University of Pennsylvania and is partially supported by the Abramson Cancer Center NCI Grant (P30 016520). The research identifier number is RRid:SCR_022376.

Conflict of Interest

The authors declare no conflict of interest.

Data Availability Statement

The data that support the findings of this study are available from the corresponding author upon reasonable request.

Keywords

drug delivery, lipid nanoparticles, nanomedicine, side effects, thrombosis

Received: November 12, 2023

Revised: February 19, 2024

Published online:

- [1] N. Chaudhary, D. Weissman, K. A. Whitehead, *Nat. Rev. Drug Discov.* **2021**, *20*, 817.
 [2] H. Parhiz, V. V. Shuvaev, N. Pardi, M. Khoshnejad, R. Y. Kiseleva, J. S. Brenner, T. Uhler, S. Tuyishime, B. L. Mui, Y. K. Tam, T. D. Madden, M. J. Hope, D. Weissman, V. R. Muzykantov, *J. Controlled Release* **2018**, *291*, 106.

- [3] M. Kim, M. Jeong, S. Hur, Y. Cho, J. Park, H. Jung, Y. Seo, H. A. Woo, K. T. Nam, K. Lee, H. Lee, *Sci. Adv.* **2021**, *7*, abf4398.
 [4] A. Akinc, W. Querbes, S. De, J. Qin, M. Frank-Kamenetsky, K. N. Jayaprakash, M. Jayaraman, K. G. Rajeev, W. L. Cantley, J. R. Dorkin, J. S. Butler, L. Qin, T. Racie, A. Sprague, E. Fava, A. Zeigerer, M. J. Hope, M. Zerial, D. W. Y. Sah, K. Fitzgerald, M. A. Tracy, M. Manoharan, V. Kotliansky, A. de Fougerolles, M. A. Maier, *Mol. Ther.* **2010**, *18*, 1357.
 [5] Q. Cheng, T. Wei, L. Farbiak, L. T. Johnson, S. A. Dilliard, D. J. Siegwart, *Nat. Nanotechnol.* **2020**, *15*, 313.
 [6] L. M. Kranz, M. Diken, H. Haas, S. Kreiter, C. Loquai, K. C. Reuter, M. Meng, D. Fritz, F. Vascotto, H. Hefesha, C. Grunwitz, M. Vormehr, Y. Hüsemann, A. Selmi, A. N. Kuhn, J. Buck, E. Derhovanessian, R. Rae, S. Attig, J. Diekmann, R. A. Jabulowsky, S. Heesch, J. Hassel, P. Langguth, S. Grabbe, C. Huber, Ö. Türeci, U. Sahin, *Nature* **2016**, *534*, 396.
 [7] D. Zhang, E. N. Atochina-Vasserman, D. S. Maurya, M. Liu, Q. Xiao, J. Lu, G. Lauri, N. Ona, E. K. Reagan, H. Ni, D. Weissman, V. Percec, *J. Am. Chem. Soc.* **2021**, *143*, 17975.
 [8] S. A. Dilliard, Q. Cheng, D. J. Siegwart, *Proc. Natl. Acad. Sci. U. S. A.* **2021**, *118*, 2109256118.
 [9] S. T. LoPresti, M. L. Arral, N. Chaudhary, K. A. Whitehead, *J. Controlled Release* **2022**, *345*, 819.
 [10] T. R. Blake, O. A. W. Haabeth, A. Sallets, R. L. McClellan, T. J. Del Castillo, J. G. Vilches-Moure, W. C. Ho, P. A. Wender, R. Levy, R. M. Waymouth, *Bioconj. Chem.* **2023**, *34*, 673.
 [11] J. C. Kaczmarek, K. J. Kauffman, O. S. Fenton, K. Sadtler, A. K. Patel, M. W. Heartlein, F. DeRosa, D. G. Anderson, *Nano Lett.* **2018**, *18*, 6449.
 [12] Y. Yan, H. Xiong, X. Zhang, Q. Cheng, D. J. Siegwart, *Biomacromolecules* **2017**, *18*, 4307.
 [13] J. W. Myerson, P. N. Patel, K. M. Rubey, M. E. Zamora, M. H. Zaleski, N. Habibi, L. R. Walsh, Y.-W. Lee, D. C. Luther, L. T. Ferguson, O. A. Marcos-Contreras, P. M. Glassman, L. L. Mazaleuskaya, I. Johnston, E. D. Hood, T. Shuvaeva, J. Wu, H.-Y. Zhang, J. V. Gregory, R. Y. Kiseleva, J. Nong, T. Grosser, C. F. Greineder, S. Mitragotri, G. S. Worthen, V. M. Rotello, J. Lahann, V. R. Muzykantov, J. S. Brenner, *Nat. Nanotechnol.* **2022**, *17*, 86.
 [14] Z. Wang, E. D. Hood, J. Nong, J. Ding, O. A. Marcos-Contreras, P. M. Glassman, K. M. Rubey, M. Zaleski, C. L. Espy, D. Gullipali, T. Miwa, V. R. Muzykantov, W.-C. Song, J. W. Myerson, J. S. Brenner, *Adv. Mater.* **2022**, *34*, 2107070.
 [15] S. Y. Fam, C. F. Chee, C. Y. Yong, K. L. Ho, A. R. Mariatulqabiah, W. S. Tan, *Nanomaterials* **2020**, *10*, 787.
 [16] X. Wu, H. Chen, C. Wu, J. Wang, S. Zhang, J. Gao, H. Wang, T. Sun, Y.-G. Yang, *Biomaterials* **2018**, *156*, 77.
 [17] A. N. Ilinskaya, M. A. Dobrovolskaia, *Nanomedicine* **2013**, *8*, 969.
 [18] C. F. Jones, R. A. Campbell, Z. Franks, C. C. Gibson, G. Thiagarajan, A. Vieira-de-Abreu, S. Sukavaneshvar, S. F. Mohammad, D. Y. Li, H. Ghandehari, A. S. Weyrich, B. D. Brooks, D. W. Grainger, *Mol. Pharm.* **2012**, *9*, 1599.
 [19] C. Oslakovic, T. Cedervall, S. Linse, B. Dahlbäck, *Nanomedicine* **2012**, *8*, 981.
 [20] K. M. de la Harpe, P. P. D. Kondiah, Y. E. Choonara, T. Marimuthu, L. C. du Toit, V. Pillay, *Cells* **2019**, *8*, 1209.
 [21] E. Fröhlich, *Curr. Med. Chem.* **2016**, *23*, 408.
 [22] L. S. Chase, M. H. Zaleski, L. J. Morrell, J. S. Brenner, *Int. J. Pharm.* **2023**, *645*, 123369.
 [23] C. T. Esmon, *Thromb. Haemost.* **2013**, *109*, 416.
 [24] M. Qiu, Y. Tang, J. Chen, R. Muriph, Z. Ye, C. Huang, J. Evans, E. P. Henske, Q. Xu, *Proc. Natl. Acad. Sci. U. S. A.* **2022**, *119*, 2116271119.
 [25] C. Maas, T. Renné, *Blood* **2018**, *131*, 1903.
 [26] Y. Sang, M. Roest, B. de Laat, P. G. de Groot, D. Huskens, *Blood Rev.* **2021**, *46*, 100733.

- [27] B. E. J. Spurgeon, M. D. Linden, A. D. Michelson, A. L. Frelinger III, *Curr. Protoc.* **2021**, 1, 178.
- [28] A. D. Blann, G. Y. Lip, *Atherosclerosis* **1997**, 128, 135.
- [29] G. Bashiri, M. S. Padilla, K. L. Swingle, S. J. Shepherd, M. J. Mitchell, K. Wang, *Lab Chip* **2023**, 23, 1432.
- [30] S. Wang, J. Zhang, H. Zhou, Y. C. Lu, X. Jin, L. Luo, J. You, *J. Controlled Release* **2023**, 360, 15.
- [31] A. D. Protopopova, N. A. Barinov, E. G. Zavyalova, A. M. Kopylov, V. I. Sergienko, D. V. Klinov, *J. Thromb. Haemost.* **2015**, 13, 570.
- [32] S.-Y. Jung, S.-M. Lim, F. Albertorio, G. Kim, M. C. Gurau, R. D. Yang, M. A. Holden, P. S. Cremer, *J. Am. Chem. Soc.* **2003**, 125, 12782.
- [33] H. Derakhshankhah, A. Hosseini, F. Taghavi, S. Jafari, A. Lotfabadi, M. R. Ejtehad, S. Shahbazi, A. Fattahi, A. Ghasemi, E. Barzegari, M. Evini, A. A. Saboury, S. M. K. Shahri, B. Ghaemi, E.-P. Ng, H. Awala, F. Omrani, I. Nabipour, M. Raoufi, R. Dinarvand, K. Shahpasand, S. Mintova, M. J. Hajipour, M. Mahmoudi, *Sci. Rep.* **2019**, 9, 1558.
- [34] Z. J. Deng, M. Liang, I. Toth, M. J. Monteiro, R. F. Minchin, *ACS Nano* **2012**, 6, 8962.
- [35] Z. J. Deng, M. Liang, M. Monteiro, I. Toth, R. F. Minchin, *Nat. Nanotechnol.* **2011**, 6, 39.
- [36] B. Savage, E. Saldívar, Z. M. Ruggeri, *Cell* **1996**, 84, 289.
- [37] Y. Qiu, A. C. Brown, W. J. Jung, Y. Sakurai, R. Mannino, D. R. Myers, R. Tran, G. Bao, T. H. Barker, W. Lam, *Blood* **2012**, 120, 384.
- [38] R. Loncar, R. B. Zotz, C. Sucker, A. Vodovnik, M. Mihalj, R. E. Scharf, *Thromb. J.* **2007**, 5, 5.
- [39] P. H. Mangin, M.-B. Onselaer, N. Receveur, N. L. Lay, A. T. Hardy, C. Wilson, X. Sanchez, S. Loyau, A. Dupuis, A. K. Babar, J. L. Miller, H. Philippou, C. E. Hughes, A. B. Herr, R. A. Ariëns, D. Mezzano, M. Jandrot-Perrus, C. Gachet, S. P. Watson, *Haematologica* **2018**, 103, 898.
- [40] R. J. Weiss, J. D. Esko, Y. Tor, *Org. Biomol. Chem.* **2017**, 15, 5656.
- [41] J. Myerson, L. He, G. Lanza, D. Tollefsen, S. Wickline, *J. Thromb. Haemost.* **2011**, 9, 1292.
- [42] P. Zeliszewska, A. Bratek-Skicki, Z. Adamczyk, M. Cieřła, *Langmuir* **2014**, 30, 11165.
- [43] H. Parhiz, J. S. Brenner, P. N. Patel, T. E. Papp, H. Shahnawaz, Q. Li, R. Shi, M. E. Zamora, A. Yadegari, O. A. Marcos-Contreras, A. Natesan, N. Pardi, V. V. Shuvaev, R. Kiseleva, J. W. Myerson, T. Uhler, R. S. Riley, X. Han, M. J. Mitchell, K. Lam, J. Heyes, D. Weissman, V. R. Muzykantov, *J. Controlled Release* **2022**, 344, 50.
- [44] O. A. Marcos-Contreras, C. F. Greineder, R. Y. Kiseleva, H. Parhiz, L. R. Walsh, V. Zuluaga-Ramirez, J. W. Myerson, E. D. Hood, C. H. Villa, I. Tombacz, N. Pardi, A. Seliga, B. L. Mui, Y. K. Tam, P. M. Glassman, V. V. Shuvaev, J. Nong, J. S. Brenner, M. Khoshnejad, T. Madden, D. Weissmann, Y. Persidsky, V. R. Muzykantov, *Proc. Natl. Acad. Sci. U. S. A.* **2020**, 117, 3405.